Stabilized photoanodes for water oxidation by integration of organic dyes, water oxidation catalysts, and electron-transfer mediators

Degao Wang[a,1], Michael S. Eberhart[a,1], Matthew V. Sheridan[a], Ke Hu[b], Benjamin D. Sherman[a,2], Animesh Nayak[a], Ying Wang[a], Seth L. Marquard[a], Christopher J. Dares[c], and Thomas J. Meyer[a,3]

[a]Department of Chemistry, University of North Carolina at Chapel Hill, Chapel Hill, NC 27599; [b]Department of Chemistry, Fudan University, 200433 Shanghai, People's Republic of China; and [c]Department of Chemistry and Biochemistry, Florida International University, Miami, FL 33199

Stabilized photoanodes for light-driven water oxidation have been prepared on nanoparticle core/shell electrodes with surface-stabilized donor–acceptor chromophores, a water oxidation catalyst, and an electron-transfer mediator. For the electrode, fluorine-doped tin oxide $FTO|SnO_2/TiO_2|$-Org1-|1.1 nm Al_2O_3|-RuP^{2+}-WOC (water oxidation catalyst) with Org1 (1-cyano-2-(4-(diphenylamino)phenyl)vinyl)phosphonic acid), the mediator RuP^{2+} ([Ru(4,4-$(PO_3H_2)_2$-2,2-bipyridine)(2,2-bipyridine)$_2$]$^{2+}$), and the WOC, Ru(bda)(py($CH_2)_{(3 or 10)}$P(O_3H)$_2)_2$ (bda is 2,2-bipyridine-6,6-dicarboxylate with x = 3 or 10), solar excitation resulted in photocurrents of ~500 μA/cm^2 and quantitative O_2 evolution at pH 4.65. Related results were obtained for other Ru(II) polypyridyl mediators. For the organic dye PP (5-(4-(dihydroxyphosphoryl) phenyl)-10,15,20-Tris(mesityl)porphyrin), solar water oxidation occurred with a driving force near 0 V.

core/shell | water oxidation | electron-transfer mediator | DSPEC | organic dye

In dye-sensitized photoelectrosynthesis cells (DSPECs), solar energy is converted into solar fuels, hydrogen, and oxygen by water splitting or carbon-based fuels by CO_2 reduction (1–4). Both are driven by the absorption of visible light by dye molecules on the surfaces of high-bandgap semiconductors (5, 6). At a photoanode for water oxidation to O_2, TiO_2 provides an accessible conduction band and redox levels that are accessible following excited-state injection (7). In DSPEC photoanodes, the redox equivalents for water oxidation are concentrated at a water oxidation catalyst (WOC) where it is used for preparing oxygen by a sequence of multielectron/multiproton reactions (8–10).

In these reactions, a limit arises from the availability of suitable chromophores. They require potentials that are suitable for water oxidation with excited states that can inject electrons into the conduction bands of appropriate semiconductor electrodes (11). In dye-sensitized solar cell applications, Ru(II) polypyridyl dyes have dominated as light absorbers, but organic dyes have also been used (12–18). For DSPECs, significant limitations can arise from the instabilities of the oxidized forms of the dyes in aqueous solution (19–21). Recently, we reported water oxidation from surfaces with organic push–pull dyes with an added WOC (19, 22). The combined light-absorber/catalyst electrodes led to water oxidation but with limited lifetimes because of the instabilities of the cationic forms of the chromophores in water, although stabilization of the dyes on the surface of TiO_2 by atomic layer deposition (ALD) of Al_2O_3 has been reported (19, 20).

Here, we extend the approach by adding an external electron-transfer mediator, RuP^{2+}, to surfaces stabilized by the addition of Al_2O_3, as shown in Fig. 1. Addition of the complex, with $E_{1/2} = 1.28V$ versus normal hydrogen electrode (NHE) for the Ru(III/II) couple in 0.1 M $HClO_4$, creates an electron-transfer pathway for transferring oxidative equivalents from the oxidized chromophore to the catalyst (23, 24).

Structures are shown in Fig. 2. On these electrodes, RuP^{2+} is a visible light absorber that competes with the organic dye, but, in the high-energy visible region of the spectrum, which is dominated

by the dye, it is a minor contributor. Preparation and characterization of the electrodes, $FTO|SnO_2/TiO_2|$-*dye*-$|Al_2O_3|$-RuP^{2+}-WOC, is described in the experiment.

As a final step in preparing working electrodes, a derivatized version of the WOC, Ru(bda)(L)$_2$ (bda is 2,2-bipyridine-6,6-dicarboxylate) L = 4-pyO($CH_2)_{(3,10)}PO_3H_2$ was added to give the final assemblies, $FTO|SnO_2/TiO_2|$-**organic dye**-$|Al_2O_3|$-RuP^{2+}-WOC. Of interest in comparing the catalysts was the role of the long-chain -$(CH_2)_{3,10}$- structure in dictating photocurrent efficiencies, Fig. 3.

In the electrode structures, -RuP^{2+}- was added as electron-transfer mediator. With RuP^{2+} in the outer layer, with a redox potential sufficient to transfer electrons away from the surface dye by oxidation to -RuP^{3+}-, the mediator provides a basis for subsequent oxidation of the external catalyst, -|-Org1$^{•+}$ -|1.1 nm $Al_2O_3|$-RuP^{2+}-WOC → -|-Org1-|1.1 nm $Al_2O_3|$-RuP^{3+}-WOC → -|-Org1-|1.1 nm $Al_2O_3|$-RuP^{2+}-WOC$^+$.

Results and Discussion

Electrode Characterization. The organic dyes have visible absorption maxima at ~400 nm, depending on the environment and substituents. Absorption manifolds can extend to ~500 nm with substituents that can vary from hydrogen to methoxide, as shown

Significance

Dye-sensitized photoelectrosynthesis cells (DSPECs) are a very promising approach to convert solar energy into chemical fuels as H_2 or reduced CO_2 species from water or CO_2. Water oxidation occurring in the photoanode, involving 4e$^-$ process, is a critical reaction for the artificial photosynthesis. Here, we inserted an electron mediator between light harvester and water oxidation catalyst. In this role it acts as a mimic for the tyrosine (Yz) between the chromophore and catalyst in PSII. The resulting assembly structures were stable for extended periods (3 h) toward water oxidation to O_2, and they also extended the chromophores used in the DSPECs for water oxidation to a phosphonated porphyrin dye.
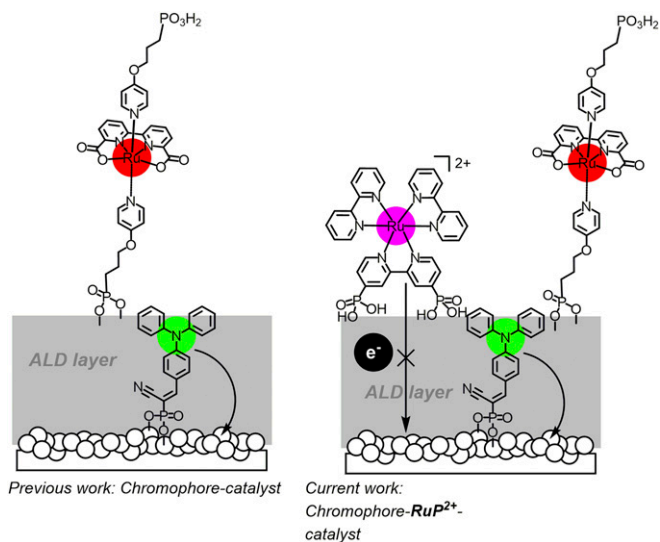
Fig. 1. (*Left*) Organic dye-chromophore catalyst assembly. (*Right*) Assembly with a Ru(II) polypyridyl, electron-transfer mediator.

in *SI Appendix*, Fig. S1 (19). As obtained by cyclic voltammetry measurements, $E_{1/2}$ values for **Org1**$^{\bullet+/0}$ and **Org2**$^{\bullet+/0}$ in aqueous 0.1 M KPF_6 are ~1.04 and 1.03 V versus NHE, with some uncertainty in the values from kinetic distortions in the voltammograms. In acetonitrile, $E_{1/2}$ values for the **Org1**$^{\bullet+/0}$, **Org2**$^{\bullet+/0}$, and **Org3**$^{\bullet+/0}$ couples are 1.23, 1.21, and 1.03 V versus NHE, respectively (19).

The influence of surface loading of **RuP**$^{2+}$ on added Al_2O_3 is shown in the UV-vis spectra in Fig. 4. Increasing the ALD-deposited Al_2O_3 overlayer from 0.36 nm to 1.1 nm resulted in enhancement of the **RuP**$^{2+}$ MCLT absorptions at ~450 nm. Further increases past 1.1 nm to 1.6 nm resulted in no further increase. Nine ALD cycles of the Al_2O_3 overlayer were equivalent to ~1.1 nm which is the approximate diameter of **Org1**.

Photoelectrochemical Water Oxidation. Water oxidation was explored in core/shell nanoparticle SnO_2/TiO_2 films with the core/shell structure assisting electron–hole separation at the SnO_2/TiO_2 interface (25–29). Surface-loaded versions of related assemblies were investigated previously (30). Based on results from earlier studies, surface loading occurs at a 2:1 ratio of **RuP**$^{2+}$ compared with the catalyst **WOC(A)** (30). With the structures of the catalysts shown in Fig. 2, and the supporting $-(CH_2)_n-$ methylene chains of 3 or 10, the catalysts are well separated from the initial oxide surface.

From the data in Fig. 5, photocurrent densities at anodes with different Al_2O_3 thicknesses, and varying amounts of -**RuP**$^{2+}$, gave similar photoresponses. In the assembly FTO|SnO_2/TiO_2|-**Org1**-|Al_2O_3|-**RuP**$^{2+}$-**WOC(A)**, there was no evidence for enhanced
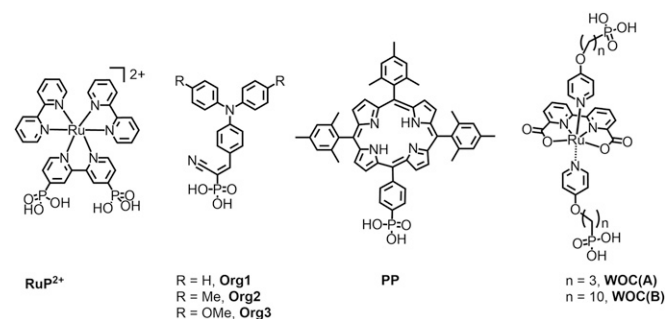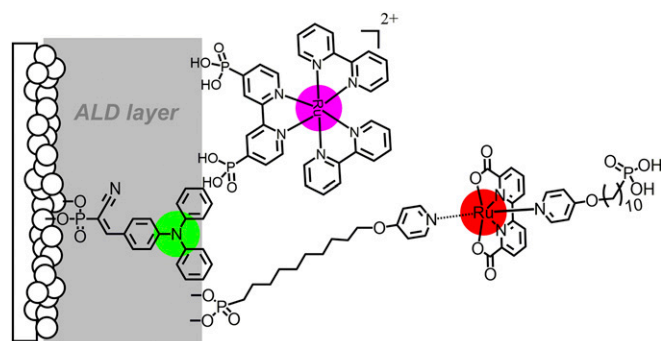

Fig. 3. Electrode configuration illustrating the $-(CH_2)_{10}-$ extended carbon chain in the catalyst.

photocurrents compared with FTO|SnO_2/TiO_2|-**Org1**-|Al_2O_3|-**WOC** (**A**) except for long-term stability. Similar configurations, but with **Org2** or **Org3** as the chromophores, in FTO|SnO_2/TiO_2|-**Org2** or **Org3**-|1.1 nm Al_2O_3|-**RuP**$^{2+}$-**WOC(A)**, gave comparable *j*-t traces (*SI Appendix*, Figs. S5 and S11) with no evidence in the photocurrent profiles for a contribution by -**RuP**$^{2+}$-.

$$(Q_{Collector}/Q_{Generator})/0.70 \times 100\% = FE(\%). \quad [1]$$

To test the stability and efficiency of the electrodes toward O_2 generation, collector–generator (C-G) experiments were carried out with a dual-electrode design described elsewhere (31, 32). The results of a 1-h illumination period with an ~1-sun intensity light source (100-mW cm^{-2} and 400-nm long-pass filter) are shown in Fig. 6. At the end of a photolysis cycle, the generator current decayed instantaneously with slower decay at generator electrode as diffusion of O_2 to the electrode occurs. Faradaic efficiencies (FE) for O_2 production were calculated from Eq. **1** with $Q_{collector}$ and $Q_{generator}$ the total charge passed at the collector and generator electrodes, respectively. The constant, 0.7, is the experimentally derived, collection efficiency for the cell, as described previously (32). In contrast to measurements on organic dyes without **RuP**$^{2+}$, the photoanodes were relatively stable over 1-h test periods with FE for O_2 production of ~100%.

Introduction of **RuP**$^{2+}$ not only improved the stability of the photoanodes, it also led to enhanced O_2 production. Addition of **RuP**$^{2+}$ resulted in enhancements in the FE for O_2 production from 43 to 100%, in *SI Appendix*, Figs. S2–S6. Similar results were obtained for assemblies with **Org2** and **Org3** as the dyes based on photocurrent and O_2 measurements, in *SI Appendix*, Figs. S7–S16.

Variations in Cell Configuration.
Dye reversal. In one series of experiments, electrodes were prepared with the position of **RuP**$^{2+}$ and the dyes reversed, FTO|SnO_2/TiO_2|-**RuP**$^{2+}$-|*x*Al_2O_3|-**Org1**. Before attaching the catalyst to the surface, three cycles (~0.36 nm) of ALD-Al_2O_3 were added to stabilize **Org1** on the surface. As shown by the data in *SI Appendix*, Figs. S17–S20, inverting the sequence of dye and mediator resulted in a slight increase in photocurrent density. However, the change in sequence caused a notable decrease in stability because of the **Org1**$^{\bullet+}$ reactivity of the cation with the solvent in water oxidation cycles. Photocurrents fell from ~1 mA/cm^2 to 65 μA/cm^2 for **FTO|SnO_2/TiO_2|-RuP^{2+}-|1.1 nm Al_2O_3|-Org1-|0.36 nm Al_2O_3|-WOC(A)** over a period of 1 h, as shown in *SI Appendix*, Fig. S20.
Dye variations. The role of other ruthenium polypyridyl complexes as mediators was investigated in films with **RuP**$^{2+}$ replaced by $[Ru(4,4'-CH_2-PO_3H_2-bpy)(bpy)_2]^{2+}$, **RuCP**$^{2+}$, and $[Ru(4,4'-PO_3H_2-bpy)(4,4'-Me-bpy)_2]^{2+}$, **RuPMe**$^{2+}$. The structures of the complexes are shown in *SI Appendix*, Scheme S2 with $E_{1/2}$ values for their
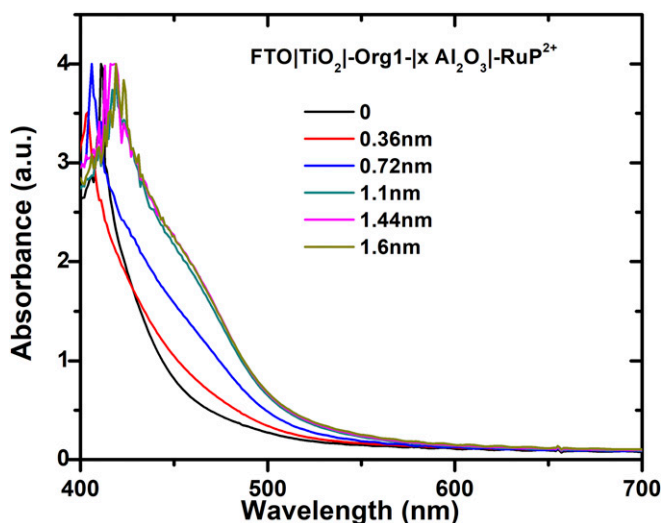

Fig. 2. Chromophore and WOC structures.

Fig. 4. UV-visible measurements on FTO|TiO$_2$|-Org1-|xAl$_2$O$_3$|-RuP^{2+}, illustrating the influence of the Al$_2$O$_3$ layer on the extent of -RuP^{2+} loading with $\lambda_{max} \sim 450$ nm. The Al$_2$O$_3$ layer was increased by ~0.12 nm per added Al$_2$O$_3$ layer. Full surface coverage occurred at nine cycles of added Al$_2$O$_3$.

Ru(III/II) couples, 1.22 and 1.19 V versus NHE in 0.1 M HClO$_4$ solution (24). From the data, *SI Appendix*, Figs. S21 and S22, after 1 h of photolysis under 1-sun illumination, a photocurrent density of 270 μA/cm^2 was obtained for FTO|SnO$_2$/TiO$_2$|-Org1-|1.1 nm Al$_2$O$_3$|-RuCP^{2+}-WOC(A) and 210 μA/cm^2 for FTO|SnO$_2$/TiO$_2$|-Org1-|1.1 nm Al$_2$O$_3$|-RuPMe^{2+}-WOC(A). As for RuP^{2+} as the mediator, addition of both complexes greatly enhanced the stabilities of the photoanodes.

Incident Photon to Current Efficiency (IPCE) measurements. The impact of RuP^{2+} on photocurrent response was also investigated by IPCE measurements with and without RuP^{2+}. Results for the electrodes FTO|SnO$_2$/TiO$_2$|-Org1-|1.1 nm Al$_2$O$_3$|-RuP^{2+}-WOC(A) are shown in Fig. 7. Based on the data, there was no evidence for participation by RuP^{2+} as a light absorber in the reactions. Related results are shown for the dyes Org2 and Org3 in *SI Appendix*, Figs. S23 and S24.
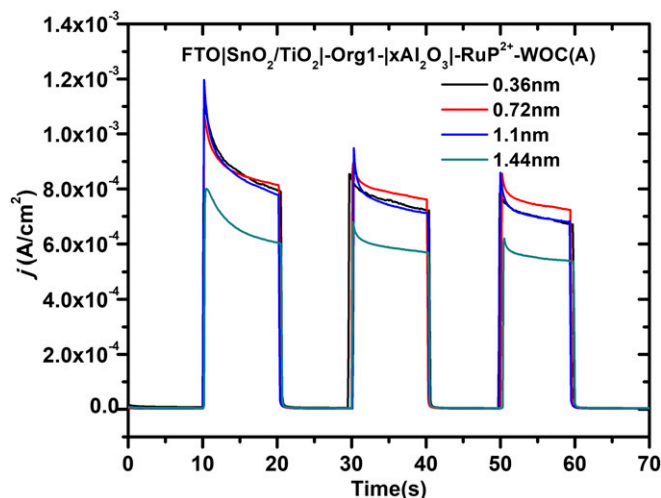
Light intensity. To explore the role of light intensity, the photoelectrochemical response of the electrode, FTO|SnO$_2$/TiO$_2$|-Org1-|1.1 nm Al$_2$O$_3$|-RuP^{2+}-WOC, as a function of incident light intensity from a 1-sun solar lamp, was also explored over range of intensities from 0.08 to 0.4 I$_o$. Based on the data in *SI Appendix*, Fig. S25, the variation with light intensity from the 1-sun incident light source was linear from 0.08 to 0.4 I$_o$, consistent with single-photon excitation and activation of the assembly.

Mechanism. A possible mechanism for the origin of the photocurrents is shown in Eqs. 2–5 with Org1 as the organic dye. In the scheme, light absorption by the organic chromophore was followed by injection from the excited state, -Org1*-. Following injection, the radical cation Org1$^{•+}$ oxidizes RuP^{2+} on the surface of the film, which in turn oxidizes the external catalyst WOC. As suggested in Eq. 4, with the addition of external RuP^{2+} on the outside of the film, injection is followed by electron transfer from the dye cation to RuP^{2+} to give the intermediate, -Org1-|1.1 nm Al$_2$O$_3$|-RuP^{3+}-WOC, with stabilization of the assembly due to the electron mediator effect of the RuP$^{3+/2+}$ couple.
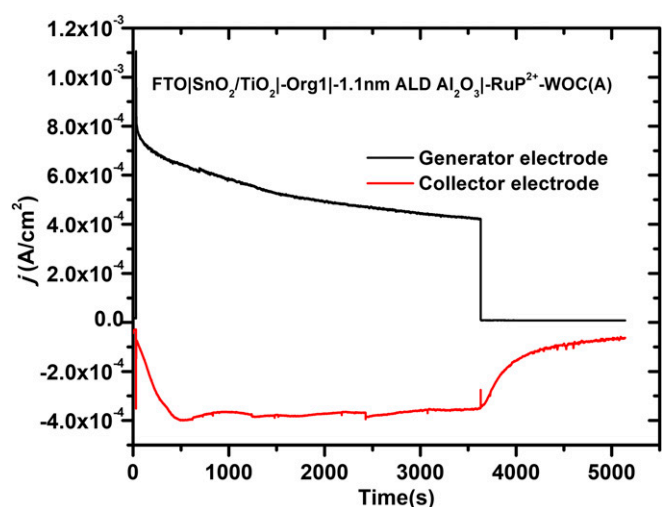
$$\text{FTO}|\text{SnO}_2/\text{TiO}_2|\text{-Org1-}|1.1\text{ nm Al}_2\text{O}_3|\text{-RuP}^{2+}\text{-WOC} + h\nu \rightarrow$$
$$\text{FTO}|\text{SnO}_2/\text{TiO}_2|\text{-Org1}*\text{-}|1.1\text{ nm Al}_2\text{O}_3|\text{-RuP}^{2+}\text{-WOC}$$

[2]

$$\text{FTO}|\text{SnO}_2/\text{TiO}_2|\text{-Org1}*\text{-}|1.1\text{ nm Al}_2\text{O}_3|\text{-RuP}^{2+}\text{-WOC} \rightarrow$$
$$\text{FTO}(e^-)|\text{SnO}_2/\text{TiO2}|\text{-Org1}^{•+}\text{-}|1.1\text{ nm Al}_2\text{O}_3|\text{-RuP}^{2+}\text{-WOC}$$

[3]

$$\text{FTO}(e^-)|\text{SnO}_2/\text{TiO}_2|\text{-Org1}^{•+}\text{-}|1.1\text{ nm Al}_2\text{O}_3|\text{-RuP}^{2+}\text{-WOC} \rightarrow$$
$$\text{FTO}(e^-)|\text{SnO}_2/\text{TiO}_2|\text{-Org1-}|1.1\text{ nm Al}_2\text{O}_3|\text{-RuP}^{3+}\text{-WOC}$$

[4]

$$\text{FTO}(e^-)|\text{SnO}_2/\text{TiO}_2|\text{-Org1-}|1.1\text{ nm Al}_2\text{O}_3|\text{-RuP}^{3+}\text{-WOC} \rightarrow$$
$$\text{FTO}(e^-)|\text{SnO}_2/\text{TiO}_2|\text{-Org1-}|1.1\text{ nm Al}_2\text{O}_3|\text{-RuP}^{2+}\text{-WOC}^+.$$

[5]

Fig. 5. Current density–time (j-t) traces over 10-s dark–light cycles for water oxidation by the electrodes, FTO|SnO$_2$/TiO$_2$|-Org1-|xAl$_2$O$_3$|-RuP^{2+}-WOC(A) with variations in x from 0 to 12 cycles at an applied bias of 0.4 V versus Ag/AgCl; pH = 4.65, 0.1 M acetate, 0.4 M NaClO$_4$.
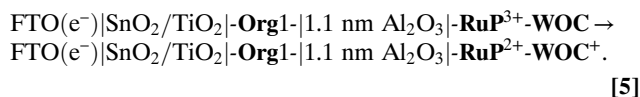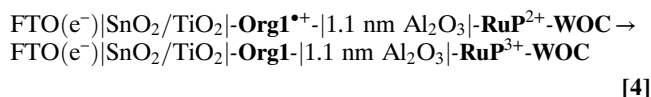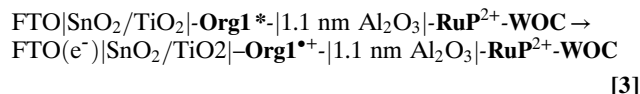

Fig. 6. O$_2$ measurements for water oxidation (black) from, FTO|SnO$_2$/TiO$_2$|-Org1-|1.1 nm Al$_2$O$_3$|-RuP^{2+}-WOC(A), on 1-cm^2 slides illuminated with 100-mW cm^{-2} white light with a 400-nm cutoff filter from 30 to 3,630 s at a bias of 0.4 V versus Ag/AgCl. The current–time response in red is for the O$_2$ collector electrode held 1 mm from the photoanode poised at −0.85 V versus Ag/AgCl; in 0.1 M acetic acid/acetate buffer at pH 4.65 containing 0.4 M NaClO$_4$.
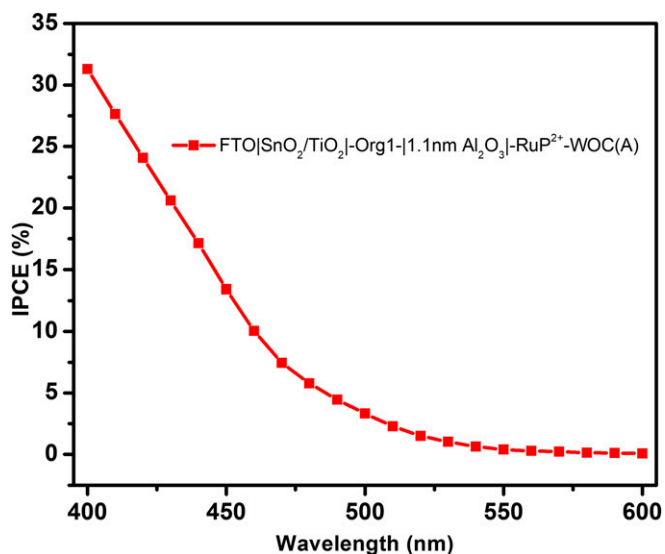
CHEMISTRY

Wang et al.

PNAS | August 21, 2018 | vol. 115 | no. 34 | 8525

Fig. 7. IPCE measurements on FTO|SnO$_2$/TiO$_2$|-**Org1**-|1.1 nm Al$_2$O$_3$|-**RuP^{2+}-WOC (A)**, at an applied bias of 0.4 V versus Ag/AgCl at pH = 4.65 in 0.1 M acetate buffer, 0.4 M in NaClO$_4$. A 400-nm cutoff filter was used to mimic the conditions in Fig. 2.

In the scheme, **RuP^{2+}** may act as an electron-transfer mediator between the oxidized dye and the external catalyst. Based on redox potentials for the **RuP$^{3+/2+}$** couple in 0.1 M aqueous HClO$_4$, and for the **Org1$^{\bullet+/0}$** couple in 0.1 M aqueous KPF$_6$, oxidation of **RuP^{2+}** to **RuP^{3+}** by **Org1$^{\bullet+}$** is nominally disfavored by ~0.2 V. There was no evidence for a buildup of **RuP^{3+}** during the experiment and we assume, that in the film structure, the reaction is either favorable or, if unfavorable, with a sufficiently low driving force that it does not inhibit catalyst activation. Based on the light-intensity experiments described above, there was also no evidence for additional steps in the mechanism involving multiphoton excitation of **RuP^{2+}** in the photocatalytic cycle.

Transient Dynamics. Transient absorption measurements were undertaken to explore excited-state processes following excitation of
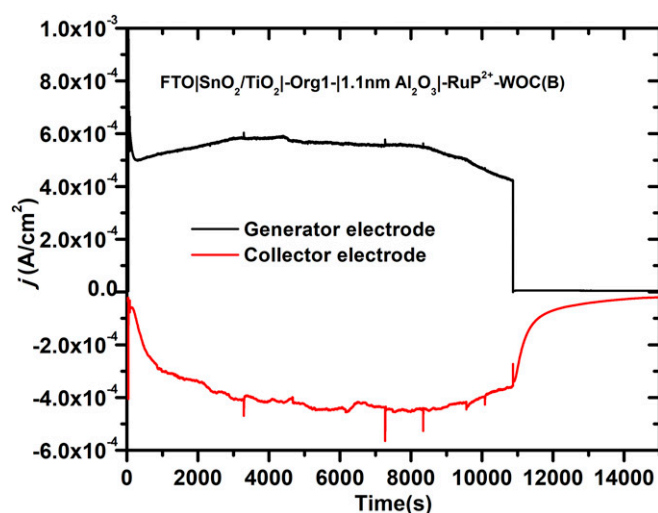

Fig. 8. O$_2$ measurements for water oxidation from (black), FTO|SnO$_2$/TiO$_2$|-**Org1**-|1.1 nm Al$_2$O$_3$|-**RuP^{2+}-WOC(B)**, on 1-cm^2 slides illuminated with a 100-mW cm^{-2} white-light source with a 400-nm cutoff filter for 180 min at a bias of 0.4 V versus Ag/AgCl. The current–time response in red was for an O$_2$ sensor electrode, 1 mm from the photoanode biased at −0.85 V versus Ag/AgCl in 0.1 M acetic acid/acetate buffer at pH 4.65 in 0.4 M NaClO$_4$.

Org1 in FTO|SnO$_2$/TiO$_2$|-**Org1**-|1.1 nm Al$_2$O$_3$, and FTO|SnO$_2$/TiO$_2$|-**Org1**-|1.1 nm Al$_2$O$_3$|-**RuP^{2+}**. In transient absorption experiments on FTO|SnO$_2$/TiO$_2$|-**Org1**-|1.1 nm Al$_2$O$_3$, the kinetics of back electron transfer from the surface to **Org1$^{\bullet+}$** occur with a half time of 5 µs following 425-nm excitation. In a second series of experiments, transient absorption measurements were conducted on FTO|SnO$_2$/TiO$_2$|-**Org1**-|1.1 nm Al$_2$O$_3$|-**RuP^{2+}**, under the same conditions, but at an excitation wavelength of 535 nm, above the absorption maximum for the organic dye. Under these conditions, **RuP^{2+}** is the dominant light absorber in the electrode. Following excitation at 535 nm only excitation of **RuP^{2+}** to give **RuP^{2+*}** was observed and it decayed with 280 ns, *SI Appendix*, Figs. S26 and S27. There was no evidence in the data for injection or for the appearance of **RuP^{3+}**.

Structural Variations.

Alkyl chain length. To further explore the role of structure in WOC, we investigated the role of distance from the surface by varying the bridge to the catalyst from –(CH$_2$)$_3$- to –(CH$_2$)$_{10}$- in FTO|SnO$_2$/TiO$_2$|-**Org1**-|1.1 nm Al$_2$O$_3$|-**RuP^{2+}-WOC(B)**. In the fully extended structure, the separation distance from the surface was ~**1.4** nm. The results of earlier experiments have shown that longer alkyl chains can lead to stabilization of the catalyst toward hydrolysis from the surface (33). Photocurrent measurements under the conditions in Fig. 5 resulted in photocurrent densities of ~0.5 mA/cm^2 which lasted for 3 h without a significant loss in photocurrent. As shown in Fig. 8, O$_2$ evolution was retained over the entire photolysis period.

Other chromophores. The electrode procedure was extended to the phosphonate derivatized, free-base porphyrin dye, 5-(4-(dihydroxyphosphoryl)phenyl)-10,15,20-Tris(mesityl)porphyrin, (**PP**), as the added chromophore, Fig. 9. Porphyrins are attractive chromophores due to their excellent light absorption in the visible but have not been effective as DSPEC water oxidation (34–37). E$_{p,a}$ for the initial **PP$^{\bullet+/0}$** oxidation wave was 1.05 V versus NHE in pH 4.65 buffer in 0.1 M acetate, 0.4 M NaClO$_4$, *SI Appendix*, Fig. S28. At this pH, electron transfer from the cation **PP$^{\bullet+}$** to **RuP^{2+}** following injection, is also disfavored by ~0.2 V.

The porphyrin was chosen as the chromophore because the potential for the **PP$^{\bullet+/0}$** couple is within 0–50 mV of the driving force for water oxidation to O$_2$ at pH = 4.65. As for **RuP^{2+}** as the electron-transfer mediator, water oxidation does occur for the **PP** chromophore. Based on the experimental data, without **RuP^{2+}** as the mediator in FTO|SnO$_2$/TiO$_2$|-**PP**-|1.1 nm Al$_2$O$_3$|-**WOC(A)**, O$_2$ production was minimal, *SI Appendix*, Fig. S29. After adding **RuP^{2+}** in a second mediator layer gives FTO|SnO$_2$/
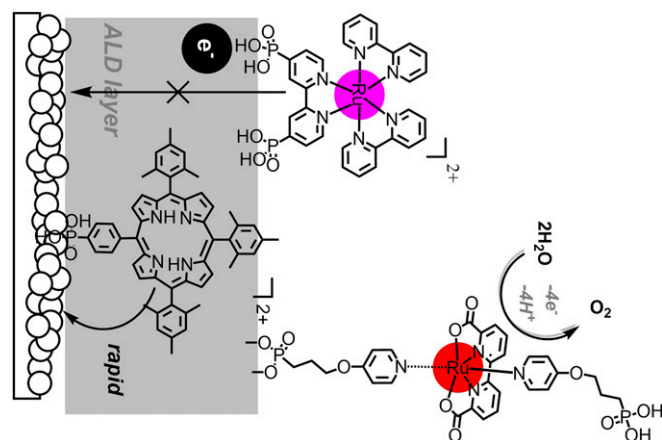
Fig. 9. Electrode configuration for the **PP** dye as the chromophore for electron transfer in FTO|SnO$_2$/TiO$_2$|-**PP**-|1.1 nm Al$_2$O$_3$|-**RuP^{2+}-WOC(A)**.

TiO_2|-**Porphyrin**-|1.1 nm Al_2O_3|-**RuP²⁺**-**WOC(A)**, photocurrents were initiated at levels of 300–400 µA/cm², *SI Appendix*, Fig. S30. Utilization of the O_2 measurement procedure after photolysis periods of 10 min gave FE of 78%. IPCE measurements on electrodes in *SI Appendix*, Fig. S31 with the porphyrin chromophore overlapped with its spectrum without evidence for a significant contribution from -**RuP²⁺**- and a dramatic example in which photoelectrochemical water oxidation is carried out with a nearly 0-V driving force.

Conclusions

The examples cited here are important in illustrating key structural features for transiently stable photoanodes for water oxidation based on three push–pull organic dyes, a derivative of the Ru(bda) catalyst for water oxidation, and an electron-transfer mediator. The key elements in the structure were the use of ALD to stabilize the surface-bound chromophores, an overlayer of Al_2O_3 for surface stabilization, and surface binding of both a WOC and the electron-transfer mediator. Addition of **RuP²⁺** as a mediator removes electrons from the organic dyes following injection stabilizing the structure, allowing for electron-transfer activation of the external catalyst. As for tyrosine in PSII, the mediator is essential in the overall structure by enabling rapid transfer of oxidative equivalents from the oxidized chromophore to the catalyst. The results are impressive with stable photocurrents observed over a 3-h photolysis period with ~100% O_2 production in the assembly FTO|SnO_2/TiO_2|-**Org1**-|1.1 nm Al_2O_3|-**RuP²⁺**-**WOC(B)**.

It is also notable that systematic variations could be made in the assembly structure. Exchange of the organic dye by **RuP²⁺** resulted in a photoanode for water oxidation, but with limited stability because of the external instability of the external radical cation of the dye. Notably, exchange of the organic chromophore by the **PP** dye also resulted in water oxidation, in a photoanode with a driving force near 0 V for O_2 evolution.

Materials and Methods

Fluorine-doped tin oxide (FTO) was purchased from Hartford Glass with a sheet resistance of 15 Ω/sq. TiO_2 films and nanoITO films were made following a well-developed recipe. The preparation of SnO_2/TiO_2 core/shell structures is described below.

Preparation of SnO_2 Films. SnO_2 paste was prepared by using colloidal suspension (15% w/v) of SnO_2 particles from Alfa Aesar. In the procedure, 1 g of acetic acid was added to 37 g of a SnO_2 colloidal solution to prepare the paste. The resulting mixture was sealed and stirred overnight. In the next step, the as-prepared solution was transferred to an autoclave (100 mL volume). The autoclave was sealed and placed in a box oven and heated for 45 min at 240° for 80 h. After the mixture was cooled, the colloids were redispersed in a sonic hall from Branson Ultrasonics for 2 min. To the dispersed mixture was added mixed polyethylene oxide (mol wt 100,000) and polyethylene glycol (mol wt 12,000). The resulting mixture was covered and

stirred a further 48 h. A doctor-blading method was utilized to make the SnO_2 film. The slides were annealed at 450° for 1 h to give 4~5-µm, 20-nm SnO_2 nanoparticle films.

ALD. ALD was performed by using a Cambridge NanoTech Savannah S200 instrument with TDMAT [tetrakis(dimethylamino)titanium] as Ti precursor. ALD was performed in a commercial reactor (Savannah S200; Cambridge Nanotech). The chamber pressure was 760 torr when exposed to air. Titanium dioxide (TiO_2) was deposited with Tetrakis (dimethylamido) titanium, Ti (NMe₂)₄ (TDMAT, 99.999%; Sigma-Aldrich), and water. The reactor chamber temperature was 150 °C. The TDMAT reservoir was kept at 75 °C (2-h preheating). ALD coating conditions were 150 °C and 20 torr of N_2 carrier gas with a sequence of 0.5-s metal precursor dose, 20-s hold, 60-s N_2 purge, 0.02-s H_2O dose, 20-s hold, 60-s N_2 purge.

After deposition of 75 cycles of TiO_2 on SnO_2 films, the slides were placed into box oven for 30 min with annealing under 450°.

ALD coating of Al_2O_3 utilized the recipe: chamber temperature 130 °C and 20 torr of N_2 carrier gas with a sequence of 0.015-s metal precursor dose, 20-s hold, 60-s N_2 purge, 0.015-s H_2O dose, 20-s hold, 60-s N_2 purge.

Preparation of Electrodes. The FTO|SnO_2/TiO_2 slides were prepared by immersing the slides into organic dye solutions (2 mM) with soaking for 2 h. For the **PP** dye, the slides were soaked in 2 mM **PP** DMSO/methanol 1:1 solution for 12 h followed by rinsing with a methanol solution. The dye-loaded slides were placed in an ALD chamber and subjected to deposition of the Al_2O_3 overlayer. After depositing the metal-oxide layer, the slides were immersed in 1 mM methanol solutions of **RuP²⁺** for an additional 24 h followed by rinsing with pure methanol. The treated slides were immersed in freshly prepared solutions of the catalyst in methanol at 3 mM for 24 h to give the final assemblies, FTO|SnO_2/TiO_2|-dye-|Al_2O_3|-**RuP²⁺**-WOC. The addition of catalyst at the end of the assembly was performed in the glovebox.

Measurements. Electrochemical and photoelectrochemical experiments were performed by using either a CH Instruments 660D potentiostat or a CH Instruments 760E bipotentiostat. A Thor Labs HPLS 30–04 light source was used to provide white-light illumination. For all indicated experiments using 100-mW cm⁻² white-light illumination, the electrochemical cell was positioned an appropriate distance from the light source to receive the indicated light intensity as measured with a photodiode (Newport), and a 400-nm cutoff filter (Newport) was used to prevent direct bandgap excitation of the semiconductor layer.

In the water oxidation experiments, a two-compartment cell with a Nafion membrane was used in a three-electrode configuration, with Ag/AgCl as the reference electrode and a Pt mesh counter electrode for H2 evolution. The experiments were carried out under N_2 at pH = 4.65 in a 0.1 M aqueous sodium acetate buffers in 0.4 M $NaClO_4$ with a 100-mW/cm² white-light source (400-nm cutoff filter) at a bias of 0.4 V versus Ag/AgCl.

1. Meyer TJ (1989) Chemical approaches to artificial photosynthesis. *Acc Chem Res* 22: 163–170.
2. Moore GF, et al. (2011) A visible light water-splitting cell with a photoanode formed by codeposition of a high-potential porphyrin and an iridium water-oxidation catalyst. *Energy Environ Sci* 4:2389–2392.
3. Youngblood WJ, et al. (2009) Photoassisted overall water splitting in a visible light-absorbing dye-sensitized photoelectrochemical cell. *J Am Chem Soc* 131:926–927.
4. Gao Y, et al. (2013) Visible light driven water splitting in a molecular device with unprecedentedly high photocurrent density. *J Am Chem Soc* 135:4219–4222.
5. Ashford DL, et al. (2015) Molecular chromophore-catalyst assemblies for solar fuel applications. *Chem Rev* 115:13006–13049.
6. Brennaman MK, et al. (2016) Finding the way to solar fuels with dye-sensitized photoelectrosynthesis cells. *J Am Chem Soc* 138:13085–13102.
7. Meyer TJ, Sheridan MV, Sherman BD (2017) Mechanisms of molecular water oxidation in solution and on oxide surfaces. *Chem Soc Rev* 46:6148–6169.
8. Duan L, Wang L, Li F, Li F, Sun L (2015) Highly efficient bioinspired molecular Ru water oxidation catalysts with negatively charged backbone ligands. *Acc Chem Res* 48:2084–2096.
9. Fielden J, et al. (2015) Water splitting with polyoxometalate-treated photoanodes: Enhancing performance through sensitizer design. *Chem Sci (Camb)* 6:5531–5543.
10. Xu P, McCool NS, Mallouk TE (2017) Water splitting dye-sensitized solar cells. *Nano Today* 14:42–58.
11. Francàs L, et al. (2017) Kinetic analysis of an efficient molecular light-driven water oxidation system. *ACS Catal* 7:5142–5150.
12. Yella A, et al. (2011) Porphyrin-sensitized solar cells with cobalt (II/III)-based redox electrolyte exceed 12 percent efficiency. *Science* 334:629–634.
13. Wu Y, Zhu W-H, Zakeeruddin SM, Grätzel M (2015) Insight into D-A-π-A structured sensitizers: A promising route to highly efficient and stable dye-sensitized solar cells. *ACS Appl Mater Interfaces* 7:9307–9318.
14. Yang J, et al. (2014) Influence of the donor size in D-π-A organic dyes for dye-sensitized solar cells. *J Am Chem Soc* 136:5722–5730.
15. Zhou N, et al. (2015) Metal-free tetrathienoacene sensitizers for high-performance dye-sensitized solar cells. *J Am Chem Soc* 137:4414–4423.
16. Pashaei B, Shahroosvand H, Graetzel M, Nazeeruddin MK (2016) Influence of ancillary ligands in dye-sensitized solar cells. *Chem Rev* 116:9485–9564.
17. Urbani M, Grätzel M, Nazeeruddin MK, Torres T (2014) Meso-substituted porphyrins for dye-sensitized solar cells. *Chem Rev* 114:12330–12396.
18. Hagfeldt A, Boschloo G, Sun L, Kloo L, Pettersson H (2010) Dye-sensitized solar cells. *Chem Rev* 110:6595–6663.

CHEMISTRY

19. Eberhart MS, et al. (2017) Water photo-oxidation initiated by surface-bound organic chromophores. *J Am Chem Soc* 139:16248–16255.

20. Alibabaei L, et al. (2017) Chromophore-catalyst assembly for water oxidation prepared by atomic layer deposition. *ACS Appl Mater Interfaces* 9:39018–39026.

21. Kirner JT, Finke RG (2017) Water-oxidation photoanodes using organic light-harvesting materials: A review. *J Mater Chem A* 5:19560–19592.

22. Wee K-R, et al. (2016) An aqueous, organic dye derivatized SnO_2/TiO_2 core/shell photoanode. *J Mater Chem A* 4:2969–2975.

23. Hanson K, et al. (2012) Structure–property relationships in phosphonate-derivatized, RuII polypyridyl dyes on metal oxide surfaces in an aqueous environment. *J Phys Chem C* 116:14837–14847.

24. Zigler DF, et al. (2016) Disentangling the physical processes responsible for the kinetic complexity in interfacial electron transfer of excited Ru(II) polypyridyl dyes on TiO_2. *J Am Chem Soc* 138:4426–4438.

25. Wang D, et al. (2017) Inner layer control of performance in a dye-sensitized photo-electrosynthesis cell. *ACS Appl Mater Interfaces* 9:33533–33538.

26. Wang D, et al. (2017) Layer-by-layer molecular assemblies for dye-sensitized photo-electrosynthesis cells prepared by atomic layer deposition. *J Am Chem Soc* 139:14518–14525.

27. Sherman BD, et al. (2017) Light-driven water splitting by a covalently linked ruthenium-based chromophore–Catalyst assembly. *ACS Energy Lett* 2:124–128.

28. Wang D, et al. (2017) Plasmon-enhanced light-driven water oxidation by a dye-sensitized photoanode. *Proc Natl Acad Sci USA* 114:9809–9813.

29. Alibabaei L, Sherman BD, Norris MR, Brennaman MK, Meyer TJ (2015) Visible photoelectrochemical water splitting into H2 and O2 in a dye-sensitized photoelectrosynthesis cell. *Proc Natl Acad Sci USA* 112:5899–5902.

30. Sheridan MV, et al. (2016) Evaluation of chromophore and assembly design in light-driven water splitting with a molecular water oxidation catalyst. *ACS Energy Lett* 1:231–236.

31. Sherman BD, et al. (2016) A dye-sensitized photoelectrochemical tandem cell for light driven hydrogen production from water. *J Am Chem Soc* 138:16745–16753.

32. Sherman BD, Sheridan MV, Dares CJ, Meyer TJ (2016) Two electrode collector-generator method for the detection of electrochemically or photoelectrochemically produced O2. *Anal Chem* 88:7076–7082.

33. Wang D, et al. (2018) Interfacial deposition of Ru(II) bipyridine-dicarboxylate complexes by ligand substitution for applications in water oxidation catalysis. *J Am Chem Soc* 140:719–726.

34. Yamamoto M, et al. (2016) Visible light-driven water oxidation using a covalently-linked molecular catalyst-sensitizer dyad assembled on a TiO_2 electrode. *Chem Sci (Camb)* 7:1430–1439.

35. Yamamoto M, et al. (2016) Visible light-driven water oxidation with a subporphyrin sensitizer and a water oxidation catalyst. *Chem Commun (Camb)* 52:13702–13705.

36. Swierk JR, et al. (2015) Metal-free organic sensitizers for use in water-splitting dye-sensitized photoelectrochemical cells. *Proc Natl Acad Sci USA* 112:1681–1686, and erratum (2015) 112:E921.

37. Materna KL, et al. (2017) Optimization of photoanodes for photocatalytic water oxidation by combining a heterogenized iridium water-oxidation catalyst with a high-potential porphyrin photosensitizer. *ChemSusChem* 10:4526–4534.